Arch. Metall. Mater., Vol. 61 (2016), No 4, p. 1931–1938

DOI: 10.1515/amm-2016-0310

Z. SWIĄTEK*,#, I. FODCHUK**

X-RAY TOPOGRAPHY OF THE SUBSURFACE CRYSTAL LAYERS IN THE SKEW ASYMMETRIC REFLECTION GEOMETRY

The technique of X ray topography with the asymmetric reflection geometry of X-ray diffraction presented in this paper as useful tool for structural characterization of materials, particularly, epitaxial thin films and semiconductor multi-layered crystal systems used for the optoelectronic devices. New possibilities of this technique for a layer-by-layer visualization of structural changes in the subsurface crystal layers are demonstrated for semiconductors after various types of surface treatment, such as chemical etching, laser irradiation and ion implantation.

1. Introduction

It is difficult to imagine the modern physical materials science without structural investigations, as long as it is precisely structure, particularly on the atomic level, that governs important properties of materials. Therefore, improvement of known methods and creation of new ones for the investigation of materials structure continues to be relevant today. The X-ray diffraction and topographic methods are effectively used in science and technology mainly due to nondestructive nature of investigations, completeness of information obtained and possibility of application for the analysis of a real structure of highly perfect crystals. In recent years, these methods have refined appreciably in the result of development of dynamical theory of X-ray scattering and diffraction, X-ray diffraction topography, X-ray optics and computer simulation [1-3]. Not the least of the factors in this alteration has been the use of synchrotron radiation. Now, from the analysis of diffraction data it became possible to obtain a far more complete spectrum of structural characteristics of materials than previously. With the modern level of computerizing the acquisition and processing of data obtained by X-ray diffraction methods, the information can be efficiently used to improve the fabrication process of electronic devices based on a system of thin crystal layers with predetermined chemical composition.

Nowadays, there exist a great number of various X-ray methods for investigating thin subsurface layers of thickness less than 0.1μm [1-20]. However, not all of them allow visualize structural changes in these layers. Unlike X-ray topographic methods, X-ray diffraction techniques provide no information on the local distribution of defects in the crystal bulk and in thin subsurface crystal layers. Topographic methods give a direct image of many types of crystal defects and may be used to estimate crystal perfection with high strain sensitivity [9-20].

Despite its simplicity, the Berg-Barret topographic method is rather efficiently used today to characterize the structural quality of semiconductor materials [1-3]. The modification of this method, which can improve considerably its sensitivity to structural distortions in thin subsurface layers, is proposed in the present paper.

2. Skew asymmetric reflection geometry of X-ray diffraction in crystal

For purposes of a nondestructive layer by layer analysis of structural changes in the subsurface layers it is worthwhile to use the so-called skew asymmetric reflection geometry of X-ray diffraction with subsequent azimuth scanning of a sample around diffraction vector $\vec{h}$ [6, 9]. This experimental scheme of X-ray diffraction opens up new opportunities for a layer by layer visualization of structural changes in the subsurface crystal layers, and also allows increasing the discrimination of strain types in the subsurface layers using a series of diffraction reflection curves [11-20].

This diffraction geometry is different from traditional schemes in that normal $\vec{n}$ to crystal entrance surface does not lie in the diffraction plane (Fig.1) [6, 7, 9].

For the case of strongly asymmetric Bragg's diffraction with a minimum entrance angle (ϕ_0) the approximate equality $\psi \approx \theta$ holds true (θ is Bragg's diffraction angle, ψ is disorientation angle of crystallographic entrance and reflecting planes), i.e. $\phi_0 \geq \phi_{kr}$ (ϕ_{kr} is critical angle of total external reflection of X-rays) [3-8]. To realize this condition is not a problem when synchrotron radiation is available. At the same time, for the characteristic radiation of X-ray tubes the values of angles $\phi_0 \sim 10^{-3}$ can be achieved very easy [9-20]. Among possible diffraction planes (*hkl*) for the proposed diffraction geometry preference should be given to those for which the difference between the values of angles θ and ψ is insignificant, i.e. $\psi - \theta \leq 1°$.

* INSTITUTE OF METALLURGY AND MATERIALS SCIENCE, POLISH ACADEMY OF SCIENCES, 25 REYMONTA STR., 30-059 KRAKÓW, POLAND
** YURIY FEDKOVYCH CHERNIVTSI NATIONAL UNIVERSITY, 2, KOTSJUBYNSKYI STR., 58002, CHERNIVTSI, UKRAINE
# Corresponding author: z.swiatek@imim.pl

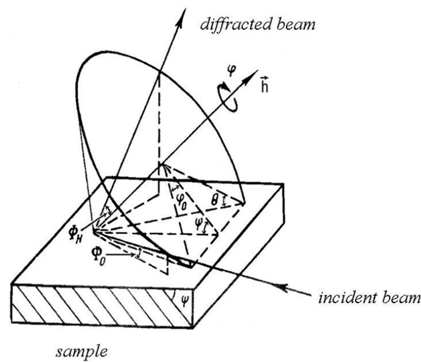

Fig.1. Schematic view of experimental set-up

Cosine of the angle between the $\vec{n}$ and the incident direction is $\gamma_0 = \cos(\phi_0)$ and between the $\vec{n}$ and the reflected direction is $\gamma_h = \cos(\phi_h)$ (Fig.1):

$$\gamma_0 = \frac{\vec{k}_0 \cdot \vec{n}}{|\vec{k}_0|},\ \gamma_h = \frac{\vec{k}_h \cdot \vec{n}}{|\vec{k}_h|},\ |\vec{k}_0| = |\vec{k}_h| = \frac{1}{\lambda}, \quad (1)$$

where λ is X-ray wavelength. By analogy to the case of a multi-beam X-ray diffraction, γ_0 and γ_h are determined as the functions of angles θ, ψ, φ [9]:

$$\gamma_{0,h} = \sin\phi_{0,h} = \pm\sin\theta\cos\psi - \cos\theta\sin\psi\cos\varphi. \quad (2)$$

where φ is the azimuth scanning angle; reading of angle φ is taken from the reference reflection corresponding to asymmetric diffraction, i.e. when wave vectors $\vec{k}_0$ and $\vec{k}_h$, and normal $\vec{n}$ lie in scattering plane.

Limiting value of azimuth scanning angle, at which the transition from Laue-diffraction to Bragg-diffraction or reverse, $\varphi \rightarrow \varphi_{0,h}$, takes place, is determined from condition of $\gamma_0 \rightarrow 0$ using ratio (2):

$$\cos\varphi_{0,h} = \pm tg\theta_B ctg\psi \quad (3)$$

There are several diffraction areas as follow from the relation (3). Bragg's diffraction corresponds to $\varphi \geq \varphi_0$, Laue's diffraction corresponds to $\varphi < \varphi_0$, is present. In the angle area $0 \geq \gamma_0 \rightarrow 0$ one can also observe the effect of total internal reflection, and in the area of angles $0 \leq \gamma_0 \leq \gamma_{0,kr}$ ($\varphi \rightarrow \varphi_{0,kr}$) both Bragg's diffraction and the effect of total external reflection of X-ray beams occur simultaneously.

The area of angles $\gamma_0 \approx \phi_0 \rightarrow \phi_{0,kr}$ represents the outstanding interest in our case of X-ray topography. From ratio (2) the value of γ_0 can be smoothly reduced to $\phi_{0,k}$ by azimuth rotation of crystal about diffraction vector $\vec{h}$ with nearly constant value of γ_h. In consequence of this the depth of X-ray penetration into subsurface crystal layers smoothly decreases due to corresponding changes of extinction length projection: $L_{ext} \rightarrow L_{kr}$ (where $L_{ext} = \frac{\lambda}{C|\chi_h|}\sqrt{\gamma_0|\gamma_h}$, C is X-ray polarization factor, χ_h is the Fourier component of the dielectric susceptibility). Simultaneously, the diffracted X-ray wave front extends in comparison with incident X-ray wave front by the value of $b = |\gamma_h|/\gamma_0$ [5,9]. It allows obtaining topograms from thin subsurface layers of a single crystal of a relatively large area without the use of scanning.

The variation range of azimuth angle φ for the angles $\gamma_0 \approx \phi_0$ ($\varphi \rightarrow j_{0,kr}$) is several degrees. It allows changing smoothly and precisely the angle of X-ray incidence on the surface, ϕ_0, using simple technical facilities. At the same time, an angle between diffracted beam and crystal surface $\phi_h = \theta + \psi$ is rather large ($\geq 80°$).

It should be noted that the effectiveness of this method, is also determined by the experimental conditions: spectral composition of radiation, the size and shape of radiation source, the distances from the source to crystal and from crystal to detector, and photoemulsion resolution in the case of using X-ray photographic film [1, 2]. The reasons related to peculiarities of X-ray scattering by local crystal volumes have an additional influence on efficiency.

3. Experimental results

Application of a skew asymmetric reflection geometry of X-ray diffraction in crystal gives an opportunity to perform selective studies of structural changes in the subsurface layers of crystalline compounds [9-20] with sufficiently small depth step (0.01-0.1 µm). Figs.2-10 show specific examples of using a skew asymmetric reflection geometry of X-ray diffraction for various crystals: a) determination of quality of mechanochemical treatment of CdTe (Fig.2, Fig.3), Ge (Fig.4), and Si (Fig.5) surfaces; b) characterization of surface relief and morphology of InSb/InSb homoepitaxial systems (Fig.6) and CdHgTe/CdTe epitaxial systems (Fig.7); c) determination of structural modifications of CdTe surface after laser irradiation (Fig.8), as well as structural changes after implantation of phosphorous ions into silicon (Fig.9). Topogram magnification is ×15.

3.1. Condition of crystals surface after various kinds of treatment

Fig.2 shows a series of topograms obtained from the subsurface layers of CdTe single crystal after chemical etching to a depth up to 100 µm. The possibility of changing L_{ext} by azimuth scanning opens up new opportunities for a nondestructive layer by layer structural analysis of the subsurface layers in such objects. Particularly it can be determined not only the main regularities of contrast formation from individual defects, but also quantitative parameters of surface roughness with high resolution. It is possible to study the following modes of defect contrast formation: orientation, adsorption and diffraction [1, 2, 9-15]. Orientation contrast is caused by inclination change of crystal surface microsegments, for instance, due to low-angle boundaries. Angular disorientation between individual crystal parts can be determined from the bends of characteristic reflexes of $K_{\alpha 1}$ and $K_{\alpha 2}$ radiation (Fig.2,c).

Adsorption contrast provided by shielding of diffracted X-ray beams by surface roughness: asperities are revealed as dark areas with cometlike shape and dark elongated areas of a regular shape correspond to twins.

Diffraction contrast results from the presence of tensile or compression strains in the area of localization of microdefects. Such a contrast on the topograms is evident as a characteristic black and white diffraction image of strain fields caused by microdefects. In the case of CdTe single crystal after chemical etching, microdefects correspond to tellurium inclusions of another phase.

In Fig.2, the length *l* of a shadow for individual surface irregularities (asperities) is related to their height, *s*, and the angle between incidence direction of X-rays and the surface, ϕ_0, by a simple ratio:

$$s = l \cdot tg(\phi_0) \approx l \cdot \phi_0 . \quad (4)$$

The height and step parameters of surface relief can be determined using measured length *l* on Fig.2, and ratio (4).

For instance, if the shadow length *l*=1 mm the height s=0.29 μm at ϕ_0=15' (a restriction is imposed by the resolution of photomaterial in detector or visualization chamber). It should be noted that the value of *l* for asperities marked by 1 and 2 in Fig.2a and Fig.2d, increase by a factor of more than 6 with a decrease of ϕ_0 from 1°30' to 0°15'. Moreover, new high-density small-scale and smaller-size dimples and asperities, for which *s* is within 0.3 to 1 μm, become identifiable. The largest height of asperity (1) is *s*≈15 μm. The bright stripe is a reflection of X-ray beams from the face of another phase inclusion (3), the smooth dark line corresponds to a twin lamella (4) projecting slightly above the surface. The bend of $K_{\alpha 1}$ reflection in Fig.2a-2b shows that there are small-angle boundaries.

Fig.3 shows topograms of CdTe crystals exposed to standard mechanochemical surface treatment. There was detected so-called "diamond background" as a system of surface microscratches that appeared in the process of mechanical surface polishing by diamond pastes (diameter of diamond powder fractions ~1 μm). The depth of its location under the surface is of the order of 0.3 μm. This damaged layer did not disappear after the process of chemical polishing to considerable thicknesses (100-150 μm) and is probably the effect of surface response (memory) to rather insignificant mechanical actions.

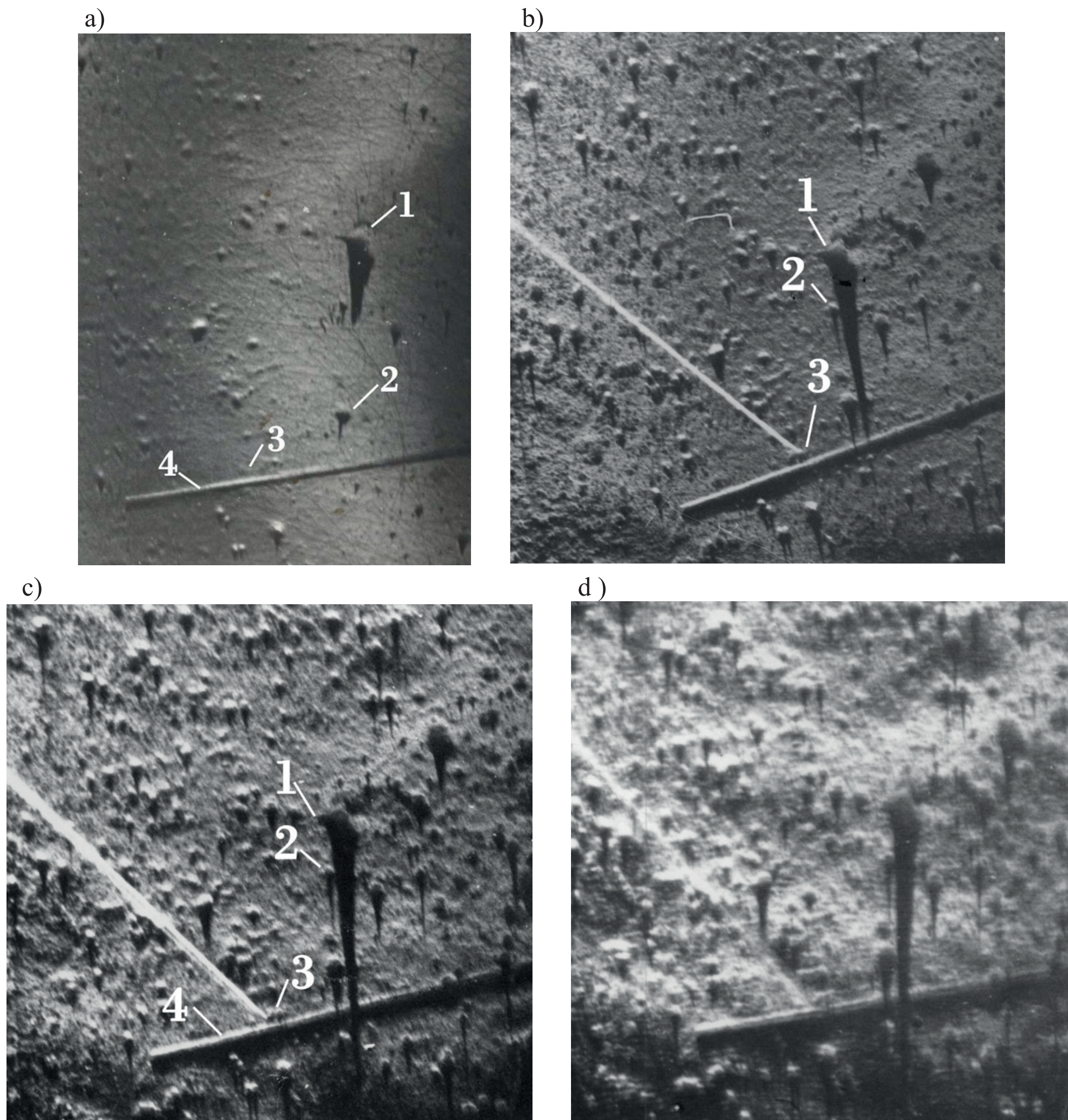

Fig. 2. Topographs of CdTe single crystal surface after chemical etching on the depth less than 100 μm [9]. Entrance surface is (111). (511) reflection, CuK_α-radiation: a) φ=23°40', ϕ_0=1°30', L_{ext}=1.89 mm; b) φ=17°40', ϕ_0=0°33', L_{ext}=1.26 mm; c) φ=16°10', ϕ_0=0°26', L_{ext}=0.88 mm; d) φ=15°40', ϕ_0=0°15', L_{ext}=0.63 μm

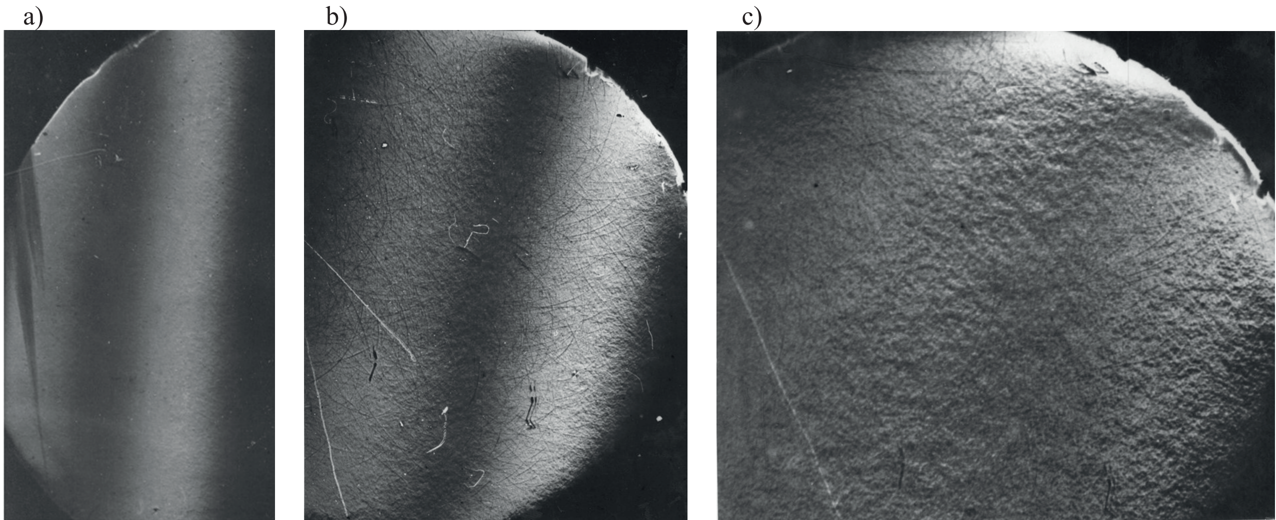

Fig. 3. Subsurface distortions in CdTe crystals after standard mechanochemical treatment of surface [10]. Entrance surface is (111). (511) reflection, CuK_α-radiation: a) ϕ_0=29°, L_{ext}=5.42 μm; b) ϕ_0=1°35’, L_{ext}=1.89 μm; c), ϕ_0=0°33’, L_{ext}=1.26 μm

Fig.4 represents topograms obtained from the surface layers of Si crystals. In addition to mechanical damages of the surface in the form of individual longitudinal microscratches, there are individual asperities (up to 1 μm) on which X-ray beams do not diffract. These asperities are caused usually by microdefects or inclusions of another phase [2].

Thus, at $\phi_0 \rightarrow \phi_{0,kr}$, there occurs a kind of X-ray optical increase of topogram resolution (by about an order of magnitude) due to a reduction of X-ray penetration depth and a stronger influence of the subsurface structural defects on the formation of diffraction pattern.

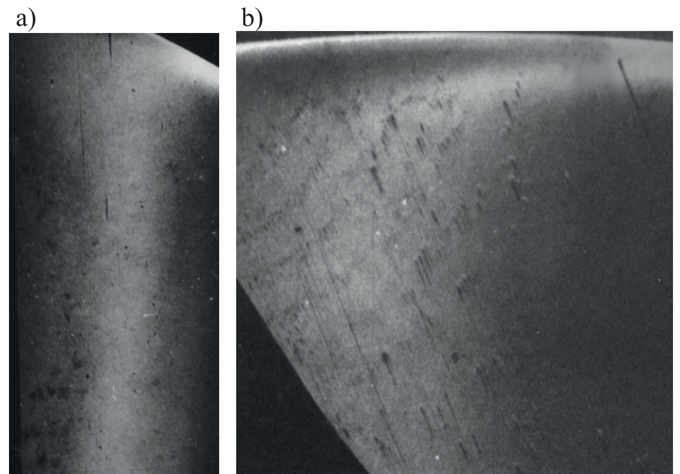

Fig. 4. Silicon. Entrance surface is (001). Skew asymmetric (331) reflection, CoKa-radiation: a) ϕ_0=3°, L_{ext}=3.4 μm; b) ϕ_0=1°, L_{ext}=1.39 μm

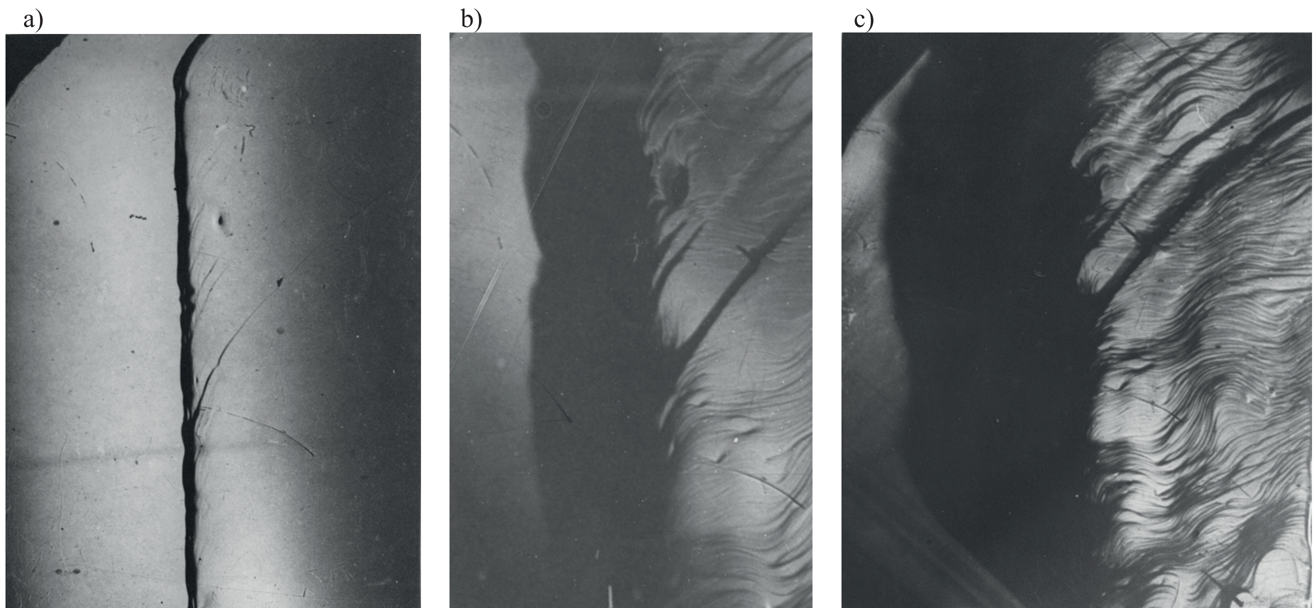

Fig.5. Surface relief of InSb/InSb homoepitaxial systems grown in hydrogen atmosphere at temperature 440°C [12, 13]. Entrance surface is (111). (511) reflection, CuK_α-radiation: a) ϕ_0=3°, L_{ext}=2.89 μm; b) ϕ_0=1°35’, L_{ext}=1.25 μm; c) ϕ_0=0°41’, L_{ext}=0.95 μm

3.2. Morphology (specific features) of epitaxial systems growth

At the present time the initial stages of epitaxial systems growth are diagnosed in sufficient detail by various techniques (X-ray diffraction, slow and fast electron diffraction, scanning electron microscopy and atomic force microscopy, etc). As a rule, morphological irregularity results from different nucleation rates, the character and rate of coalescence on different segments of substrate surface, surface relief irregularity, etc. Some growth mechanisms cause its own unique features of morphological phase orientation, structural and substructural transformations that occur during film formation. Express diagnostics of these changes can produce a significant effect on the improvement of fabrication process of such epitaxial systems with pre-assigned properties [10, 13].

Fig.5 shows topograms of InSb/InSb homoepitaxial systems obtained on the undoped substrates by liquid phase epitaxy method in a horizontal mode. Layer growth in hydrogen atmosphere was performed at temperatures 440-480°C. The resulting layers had n-type conductivity. In the majority of cases surface morphology was far from being perfect and had rather complex relief.

The use of a skew asymmetric diffraction enabled us to promptly determine the parameters of film surface relief: the height of growth steps (e.g., in Fig.6 their height is from 0.5 to 2 μm), their density (~19 per 1 mm), the distance between them (from 100 μm to 210 μm), as well as the preferred orientation [$\bar{1}$10].

3.3. Laser irradiation of CdTe surface

The surface of CdTe was irradiated by pulsed laser radiation (pulse duration $\tau=2\cdot10^{-8}$ s, energy 5 J/cm^2. Region I (Fig.6), as compared to region II, was irradiated twice. The entrance surface is (111). Reflection (511) of CuK$_\alpha$-radiation is used.

For region I the radiation diffracted by the substrate is completely absorbed in the amorphized layer at the angle ϕ_0=2°10'. In this case the thickness of amorphized layer is commensurate with the X-ray extinction length $L_{ext}\approx$2.5 μm. For region II total absorption takes place already at the angles ϕ_0=1°20', i.e. the thickness of a strongly damaged subsurface layer is $L_{ext}\approx$1.89 μm.

3.4. Ion implantation

For practical application of ion implantation it is important to have information on the set of defects and the amorphicity of surface layer. To reveal the distribution of stresses arising in the bulk crystal and in the subsurface crystal layers after implantation and subsequent annealing, one can also advantageously use this topography geometry [14-16].

Fig.7 shows topograms of silicon crystal after phosphorous ion implantation (E=180 keV, dose $Q=10^{15}$ ion/cm^2). Here again, we can choose the angles φ, at which the extinction length L_{ext} will be less or equal to the thickness of ion-damaged layer. Besides, the figure obviously demonstrates structural changes with thickness in the subsurface layers irradiated by phosphorus ions with formation of active heteroboundary. This is evidenced in Fig.7,b by double image of reflex K_{a1} obtained from the upper and lower parts with respect to implanted crystal layer.

The effective depth of localization of considerable damages of the subsurface layer, as it follows from the analysis of topogram and rocking curves, lies within 0.2 to 0.4 μm. This almost corresponds to the mean free path of phosphorous ions with such energies and doses. The elastic strain range extends to a depth of 1.0 μm. Maximum strain value of deformed layer is ~$1.6\cdot10^{-3}$. Radiation defects in a transient crystalline area underlying the surface distorted layer cause the appearance of positive lattice strains ~$4\text{-}5\cdot10^{-3}$. The amorphized layer is ~0.2 μm thick, and the thickness

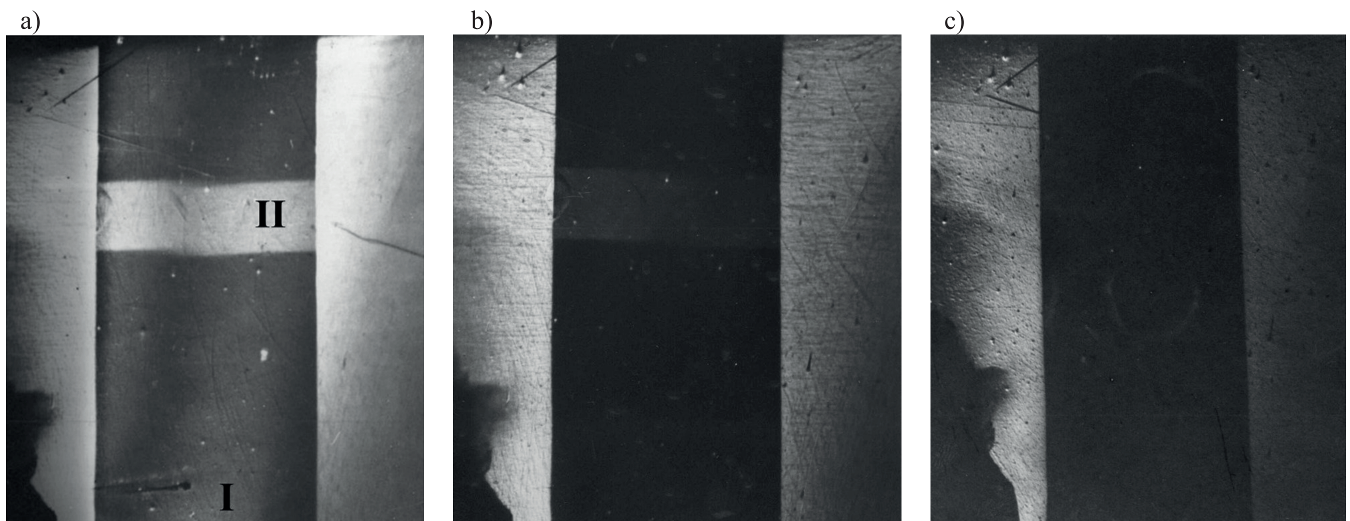

Fig. 6. Surface of CdTe, irradiated by pulsed laser radiation [10]. Entrance surface is (111). (511) reflection, CuK$_\alpha$-radiation: a) φ=35°, ϕ_0=4°20', L_{ext}=3.53 μm; b) φ=30°, ϕ_0=2°10', L_{ext}=2.5 μm; c) φ=22°0', ϕ_0=1°20', L_{ext}=1.89 μm

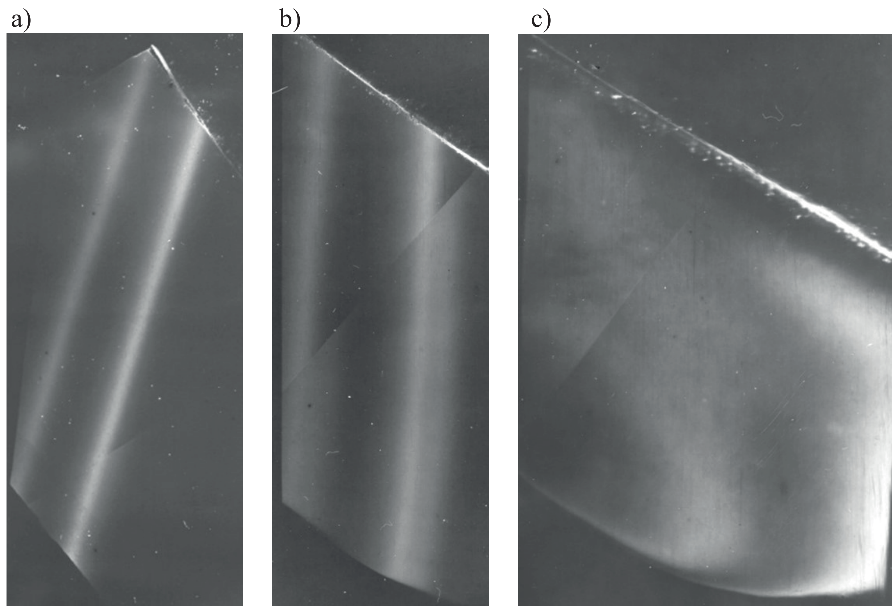

Fig. 7. Silicon. Entrance surface is (001). Skew asymmetric (331) reflection, CoK_α-radiation. The energy is E=180 keV, and dose of implantation of phosphorus ions is $Q=10^{15}$ ion/cm^2: a) L_{ext}=0.94µm, b) 0.65µm, c) 0.25 µm

of a transient layer between the amorphous region and crystal is ~0.2-0.4 µm.

Topograms in Fig.8 testify to structural features of the surface of $Cd_{1-x}Hg_xTe$ (x=0.19) epitaxial layers grown on CdTe substrates. Characteristic images on the topograms suggest compositional thickness inhomogeneity, considerable stresses in the layer and misfit dislocation systems arising in the layer-substrate transient area. These dislocation systems are shown as closed triangles in (111) plane whose sides are dislocation lines with the Burgers vectors of the type $\vec{b} = \frac{a}{2}\langle 110 \rangle$.

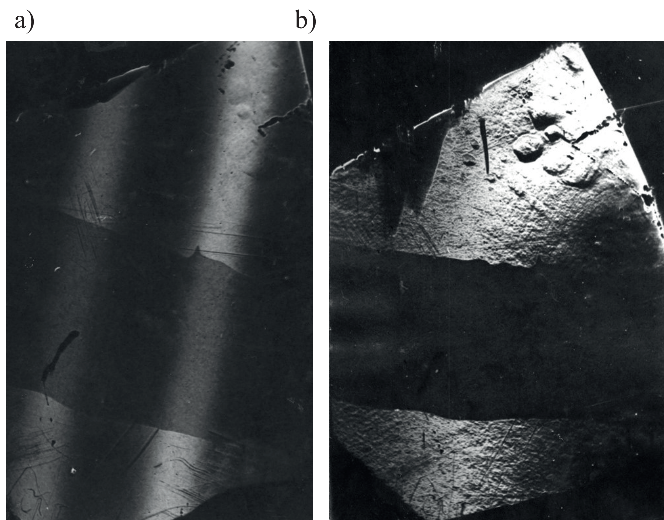

Fig. 8. Morphology and structural change of the surface of $Cd_{1-x}Hg_xTe$/CdTe epitaxial layers after implantation by As ions (E=100 keV, $D_1=10^{15}$ ion/cm^{-2}) [12]. Entrance surface is (111). (511) reflection, CuK_α-radiation: a) ϕ_0=3°, L_{ext}=1.44 µm, b) ϕ_0=0°41', L_{ext}=0.75 µm

From the analysis of topograms (Fig.8) and rocking curves it follows that the effective depth of localization of considerable damages of the subsurface layer (dark transverse stripe) lies within 0.6 to 0.75 µm. This corresponds to the free path of As ions with such energies and doses [17-20].

4. Conclusions

The represented X-ray diffraction technique in grazing geometry opens up new opportunities for a layer by layer visualization of structural changes in the subsurface crystal layers. In this topography geometry the topogram resolution increases (similar to X-ray optics) by about an order of magnitude due to a reduction of X-ray penetration depth and powerful influence of the subsurface structural defects on the formation of diffraction pattern.

Implementation of X-ray skew asymmetric topography provides a way to obtain different defect projections on the entrance crystal surface in the same (*hkl*) reflex. This gives possibility:

- to select optimal experiment geometry for the most complete interpretation of defect type, to study its orientation and corresponding elastic strains, the character of strain field distribution;
- to readily estimate the degree of structural disordering of surface layers under different external influences (laser irradiation, ion etching, ion implantation, etc.);
- to investigate the main features of X-ray diffraction contrast formation, as well as to perform quantitative diagnostics of surface relief, i.e. to estimate the height and step parameters of the asperities.

REFERENCES

[1] D. Keith Bowen, Brian K. Tanner, High Resolution X- Ray Diffractometry and Topography, 1998 Taylor & Francis, Ltd.

[2] A. Authier, Dynamical Theory of X-Ray Diffraction, 2001 Oxford University Press, New York.

[3] A.M. Afanas'ev, P.A. Alexandrov, R.M. Imamov, X-ray Diffraction Diagnostics of Submicron Layers, 1989 Nauka, Moscow.

[4] T. Bedynska, Phys. status solidi A. **19**, 365-372 (1973).

[5] F. Rustichelli, Phil. Mag. 31, 1-15 (1975).

[6] O. Brummer, H.R. Hoche, J. Nieber, Phys. Stat. Sol. A. **33**, 587-593 (1976).

[7] O. Brummer, H.R. Hoche, J. Nieber, Phys. Stat. Sol. A. **37**, 529-536 (1976).

[8] J. Hartwig, Exp. Tech. Phys. **26**, 535-546 (1978).

[9] S.A. Kchevetskiy, Yu.P. Stetsko, I.M. Fodchuk, I.V. Melnichuk, V.S. Poljanko, Ukr. J. Phys. **30** (3), 344-348 (1990).

[10] I.M. Fodchuk, O.S. Kchevetskiy, Metallophys. **14** (5), 57-62 (1992).

[11] S.A. Kchevetskiy, A.M. Raransky, I.M. Fodchuk, Metallophys. **16** (4), 66-70 (1994).

[12] I.M. Fodchuk, A.M. Raransky, A.V. Evdokimenko, X-Ray Diffraction Optics of the Submicron Surface Layers. Proc. SPIE.- Bellingham, 2647, 385-388 (1995).

[13] I.M. Fodchuk, A.M. Raransky, A.V. Evdokimenko, Inorg. Mater. **31** (10), 1669-1675 (1995).

[14] Z.T. Kuznizkii, R. Ciach, Z. Swiatek, A.M. Raransky, I.M. Fodchuk, P.M. Gorley, D.V. Kadelnik, Inorg. Mater.+ **36** (5), 615-618 (2000).

[15] J.T. Bonarski, M. Zehetbauer, Z. Swiatek, I.M. Fodchuk, I. Kopacz, S. Bernstorff, H. Amenitsch, Opto-Electron. Rev. **8** (4), 323-327 (2000).

[16] I.V. Litvinchuk, Z. Swiatek, I.M. Fodchuk, Metallofiz. Nov. Tekn.+ **27** (8), 71-82 (2004).

[17] R. Zaplitnyy, T. Kazemirskiy, I. Fodchuk, Z. Swiatek, Phys. Stat. Sol. A. **204** (8), 2714-2720 (2007).

[18] R.A. Zaplitnyy, T.A. Kazemirskiy, I.M. Fodchuk, A.P. Vlasov, O.Yu. Bonchyk, A. Barcz, P.S. Zieba, Z. Swiatek, W. Maziarz, Proc. of SPIE 7008, C1-C5 (2008).

[19] A. Vlasov, J. Bonchuk, I. Fodchuk, R. Zaplitnyy, A. Barcz, Z. Swiatek, L. Litinska-Dobrynska, P. Zieba, E. Bielanska, J. Guspiel, Arch. Metall. Mater. **52** (12), 445-451 (2007).

[20] A.P. Vlasov, O.Yu. Bonchyk, S.G. Kiyak, I.M. Fodchuk, R.M. Zaplitnyy, T. Kazemirskiy, A. Barcz, P.S. Zieba, Z. Swiatek, W. Maziarz, Thin Solid Films **516** (22), 8106-8111 (2008).